THE INTERACTION OF TIP LEAKAGE FLOW WITH INCOMING FLOW IN A COMPRESSOR CASCADE

M. W. Leitner, M. Zippel, S. Staudacher
Institute of Aircraft Propulsion Systems
Stuttgart University
Pfaffenwaldring 6, D-70569 Stuttgart
Germany

Abstract

Tip leakage flow has a very strong influence on the flow field in axial compressors. It is disadvantageous to the efficiency and mass flow stability. The interaction of the tip leakage flow with the incoming flow in a linear compressor cascade is investigated on a water channel. Tip clearance width, angle of incidence, and Reynolds number are varied systematically. To study the flow, we considered the movement of inked fluid elements in space and time. A detailed research of the area of interaction is carried out under stable and unstable flow conditions.

1. NOMENCLATURE

t	tip clearance	m
h	blade hight	m
C	chord	m
S	blade pitch	m
A	cross section area	m^2
σ	solidity	-
r	distance in radial direction	m
p	static pressure	Pa
T	static temperature	K
ρ	density	kg/m^3
η	dynamic viscosity	Pa s
v	velocity	m/s
c	absolute velocity	m/s
w	relative velocity	m/s
u	blade speed	m/s
α	flow angle from axial	°
β	flow angle from axial (rotating frame of reference)	°
i	incidence angle	°
$\dot{m}$	mass flow	kg/s
Φ	flow coefficient	-
Re	Reynolds number	-
C_p	static pressure coefficient	-
Γ	circulation	m^2/s

Subscripts

ax	axial direction
t	total
L	leakage flow
H	horseshoe vortex
1	inlet
2	outlet

2. INTRODUCTION

The rotor tip clearance in an axial compressor enables the free rotation of the rotor blade row. However, the pressure difference between the pressure and the suction side of the rotor blades drives a leakage flow across the tip clearance. The tip leakage flow has a very strong influence on the flow field in axial compressors. The leakage flow influences the boundary layers and interacts with the passage flow. Partly blockage of the channel cross section is an effect. Additionally, discrete phenomena as the horse shoe vortex and the passage vortex interact strongly with the tip leakage flow at the casing. The resulting aerodynamic losses are a considerable part of the total losses. The tip leakage flow is disadvantageous to the efficiency and stability of axial compressors. This depends on the tip clearance width. The understanding of the complex 3D flow pattern interaction will allow the optimization of gap width and blading. This is necessary for the reduction of the overall losses and hence for the optimized efficiency and stability of modern compressors.

We visualized this complex flow pattern interaction exemplarily in a water flow channel. All experimental results were obtained in a linear cascade comprising five blades. The interaction of the tip leakage flow with the incoming flow in the cascade is investigated at 2% and 4% of chord tip clearance (see Fig. 1). These clearances are representative of those that can occur in a multistage compressor [1]. Moreover, we investigated the flow at various angles of incidence and Reynolds numbers. The tip clearance is altered by a height-adjustable plate. The angle of incidence is altered by a turning of the cascade. An ideal inflow of the cascade can be guaranteed even at high incidence. To study the flow, we considered the movement

of inked fluid elements in space and time. The flow structures and vortex behavior are observed under various conditions.

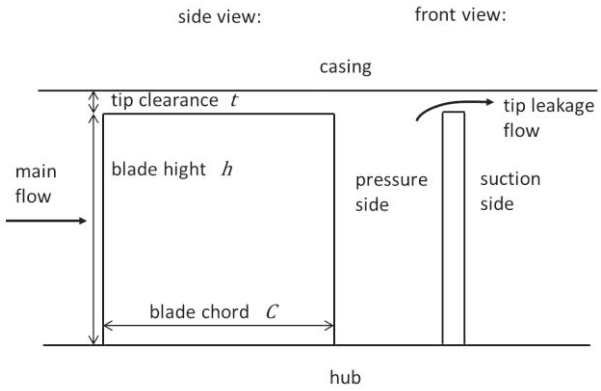

Fig. 1 Sketch of the blade with the tip leakage flow

3. BACKGROUND

Tip leakage flow is an important research topic for turbomachinery designers. This is because the tip clearance is recognized to be disadvantageous to both the efficiency and stability of axial compressors [1]. Since the study of Rains [2], who had used a three stage axial water pump to examine the tip flow, many studies has been done. Detailed measurements of the tip clearance flow have been made in axial compressors with various tip clearances, e.g. [3–6]. It has been shown that there are two distinguishable flow zones in the blade tip region: the leakage flow region and the incoming flow region.

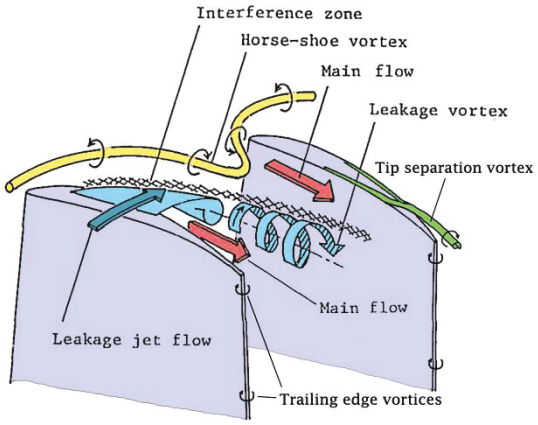

Fig. 2 Flow phenomena at the tip region of the blades [3]

The fluid dynamic phenomena near the casing are illustrated in Fig. 2. The tip leakage flow rolls up into a vortex. Additionally, a horseshoe vortex appears in the upstream of the incoming flow for every tip clearance. A substantial proportion of the total losses arises from the blade tip region [3].

Storer and Cumpsty have done measurements, simple calculations, and numerical solutions in a linear cascade with tip clearance [1]. They demonstrated that the mechanism of tip leakage is primarily inviscid. Rains proposed that incompressible tip leakage flow could be calculated by simple application of the Bernoulli equation for a given pressure difference across the blade tip [2]. Consequently, Storer and Cumpsty [1] derived the leakage velocity normal to the camber line v_L accordingly to the ideal flow model of Rains as:

$$(1)\quad \frac{v_L}{v_1} = \sqrt{C_{p\ \text{pressure side}} - C_{p\ \text{suction side}}}$$

The static pressures near the tip of the blade are quoted as the static pressure coefficient C_p

$$(2)\quad C_p = \frac{p - p_1}{p_{t1} - p_1}$$

An experimental result of Storer and Cumpsty [1] is shown in Fig. 3. The pressure distribution near tip may change significantly from that near midspan. With 4 % of chord tip clearance the maximal pressure gradient is near 50 % chord. Hence the maximal tip leakage mass flow will be near 50 % chord.

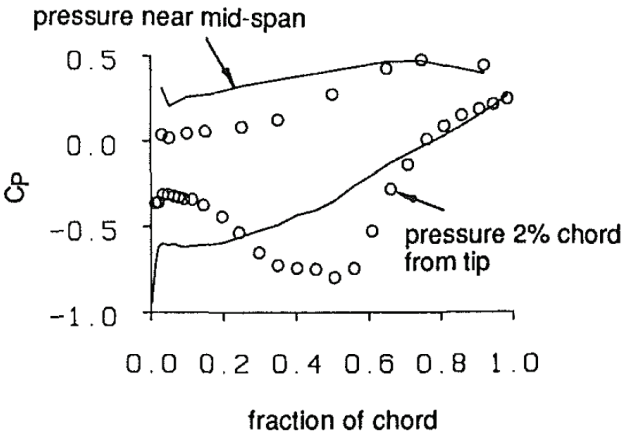

Fig. 3 Blade pressure distribution with 4 % of chord tip clearance, from Storer et al. [1]

The overall magnitude of the tip leakage flow is strongly related to the aerodynamic loading of the blades. Hence, the static pressure field near the tip of the blade is the essential aerodynamic input, necessary to predict the overall tip leakage flow.

Attempts to control instability phenomena in axial compressors have pointed to the importance of understanding the underlying fluid dynamics of the rotating stall inception process [7]. In literature two modes of stall inception are described. The long length scale or “modal” stall inception and the short length-scale or “spike” stall inception. Many axial compressors, however, exhibit spike stall inception which is as yet not fully understood [7]. But it is known that

the tip leakage flow can be responsible for the spike stall inception. This occurs at high blade loading or low flow coefficients. The flow coefficient Φ is defined as the ratio of the axial component of the flow velocity to the blade speed:

(3) $$\phi = \frac{c_{ax}}{u}$$

A numerical study of the fluid dynamic phenomena that link tip leakage flow to the formation of spike rotation stall disturbances has been carried out by Vo [8]. He proposed two criteria for tip leakage blockage behavior which are associated with the tip leakage flow:

- Alignment of the interface between the incoming flow and the tip leakage flow with the rotor leading edge plane,
- Tip leakage backflow from adjacent blade passages at the trailing edge below blade tip.

By reducing the flow coefficient, the tip clearance flow blockage grows, until the tip blockage reaches the hub and rotating stall incepts [8].

A local stall inception criterion, similar to the first criterion of Vo, is formulated by Hoying et al. [9]:

- Tip vortex trajectory perpendicular to the axial direction (see Fig. 4).

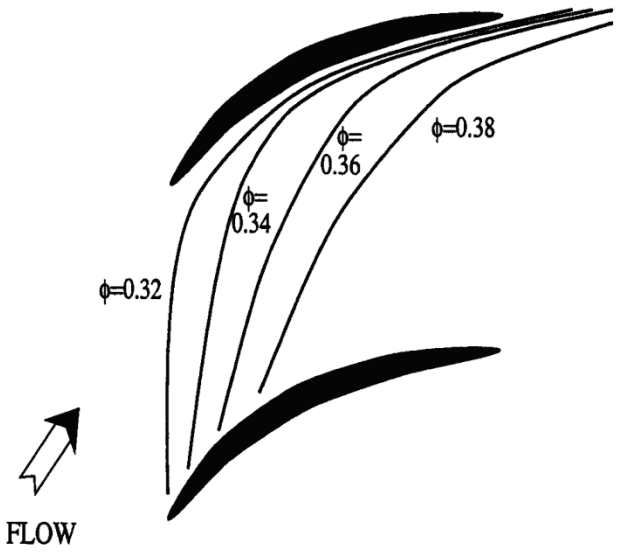

Fig. 4 Trajectories of the tip clearance vortex for different flow coefficients [9]

Fig. 4 shows the stable trajectories at four different flow coefficients from high flow (Φ=0.38) to near stall (Φ=0.32). As a consequence of the reduction of the flow coefficient the tip leakage vortex trajectory becomes closer to perpendicular to the axial direction. These results are based upon computational studies, carried out by Hoying et al. [9].

Furukawa et al. [10], however, found that the tip leakage vortex breakdown plays a major role at near stall conditions. The Navier-Stokes flow simulations show that a leakage vortex breakdown occurs inside the rotor at a lower flow rate than peak pressure rise operating condition (Φ=0.37). The onset of breakdown causes significant changes in the nature of the tip leakage vortex (see Fig. 5). Large expansion of the vortex has an extremely large blockage effect extending upstream of the leading edge. This has a significant effect on the onset of stall.

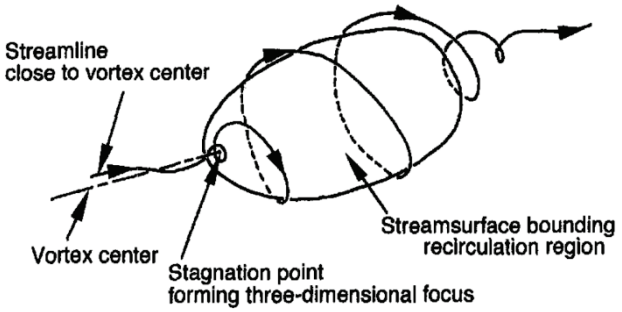

Fig. 5 Flow topology of vortex breakdown [10]

Different spike stall inception criteria are proposed by different authors. By visualizing the flow in the tip blade region, a detailed insight in the formation of the tip leakage flow, and the interaction with the incoming flow will result. As the tip leakage flow can be responsible for the spike stall inception, criteria for the inception of instable flow conditions can be found in the compressor cascade.

4. WATER CHANNEL AND EXPERIMENTAL SETUP

The experimental study used the water channel at the Institute of Aircraft Propulsion Systems of the University of Stuttgart. A schematic design of the water channel is shown in Fig. 6. Water circulates in a closed circuit. A pump delivers it through a pipe to a reservoir, from where it continues through downpipes to the main basin. This arrangement reduces the influence of the fluctuating pump flow rate. For reducing turbulence, the water passes through a calming section. It consists of a combination of sieves and honeycombs. Afterwards, the water is accelerated through a nozzle and enters the measuring section. After leaving the measurement section, the water enters a collecting basin. The collecting basin leads the water to a water tank, from which the pump is supplied.

A camera installed vertically above the measuring section allows the recording of frames. A second camera is installed horizontally at the side of the measuring section. Hence, the flow phenomena can be simultaneously observed from two orthogonally orientated directions (see e.g. Fig. 11).

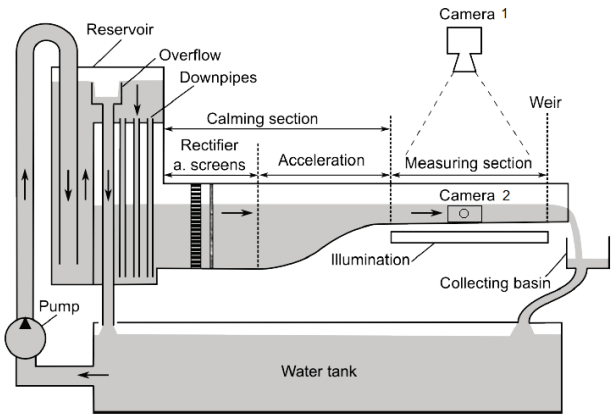

Fig. 6 Schematic design of the water channel [11]

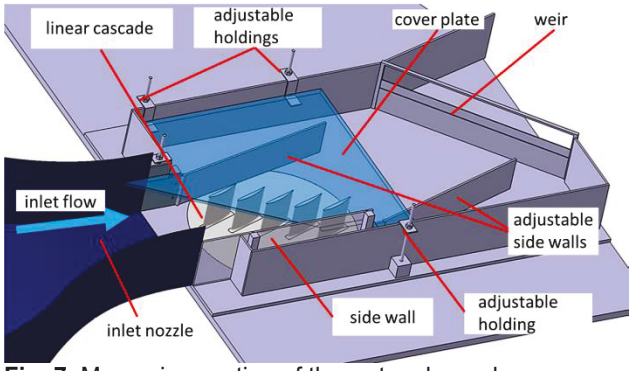

Fig. 7 Measuring section of the water channel

For that purpose, color is added to the flow to observe the flow in its course. Tough pigment is added at walls and blades. Shear forces carry the dye and reveal flow traces. When inserting dye through probes, the dye has the same density than the surrounding water. The dye is part of the flow and reveals streaklines. These visualization methods are detailed described by Vogt and Zippel (see [12]).

The measuring section is shown in Fig. 7. It comprises the linear cascade with five blades as shown in Fig. 8. The cascade is mounted on a circular plate. We designed the measurement section for a variation of the angle of incidence and the tip clearance. The inlet flow angle of the cascade can be easily altered by turning the circular plate. On water level is a transparent cover plate with vertically adjustable holdings. The height of the cover plate defines the tip clearance.

Flow conditions within the measuring section are set by a weir, in a way which takes care that during a series of measurements the overall mass flow and the water height remain constant. Therefore, for each series of measurements the same average inlet flow velocity into the measuring section is given. On this average inlet flow velocity v an average Reynolds number is established:

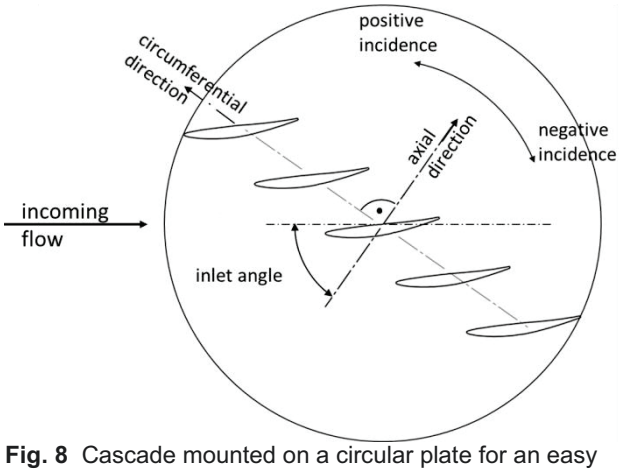

Fig. 8 Cascade mounted on a circular plate for an easy adjustment of the angle of incidence

$$(4) \quad Re = \frac{\rho v C}{\eta}$$

The characteristic length, included in the Reynolds number, is the chord length C of the blade. It is also used to create a dimensionless tip clearance. The tip clearance is formulated as per cent of chord.

The periodicity of the flow was controlled by adjustable side walls. This setup is adequate because it is only necessary to achieve the required flow conditions about the central blade. For high incidence angles we additionally used a flap to support the strong deflection of the flow in the side wall region.

Because water has a higher viscosity than air, no Reynolds number similarity can be achieved in the water channel. However, it can be assumed that the basic structure of the secondary flow don't change even at considerably higher Reynolds numbers than in the water channel [12]. Nevertheless, the effect of different Reynolds numbers on the local propagation of the flow phenomena can be analyzed.

We designed a NACA-65 profile and used it for the blades of the linear cascade. The NACA-65 is a standard compressor profile. A circular arc is used to define the camber line. The thickness distribution is added symmetrically about the camber line according to Cumpsty [13]. The maximum thickness is 10% of chord. The leading edge radius is 0.687 % of chord; the trailing edge radius is 0.8 % of chord.

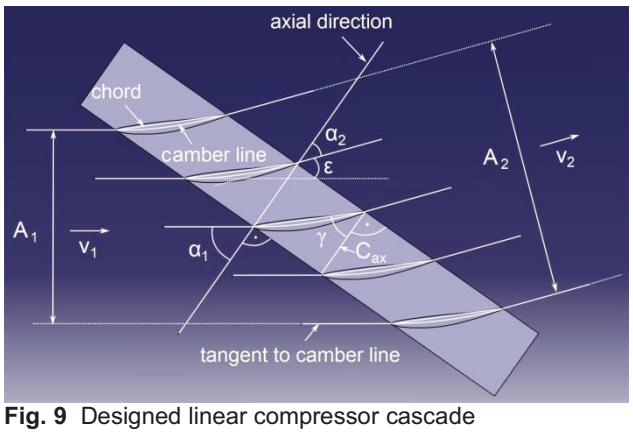

Fig. 9 Designed linear compressor cascade

Fig. 9 shows the cascade as it is designed. According to Cumpsty the diffusion factor DF = 0.45 is a typical design value [13]. An overview over the cascade design data presents Table 1.

Design parameters	
Diffusion Factor DF	0.45
de Haller Number dH	0.742
blade chord C	100 mm
blade hight h	100 mm
inlet angle α_1	55°
outlet angle α_2	39.37°
turning angle ε	15.6°
stagger angle γ	47.19°
axial chord C_{ax}	68 mm
pitch S	74.9 mm

Table 1 Design data of the linear cascade

The linear cascade can be considered as a model of an axial compressor blade row. To regard the rotating frame of reference, we introduce a relative flow angle β and a relative velocity w. We assume the inlet flow is axial. Hence, the absolute inlet rotor velocity is:

(5) $c_1 = c_{\mathrm{ax1}}$

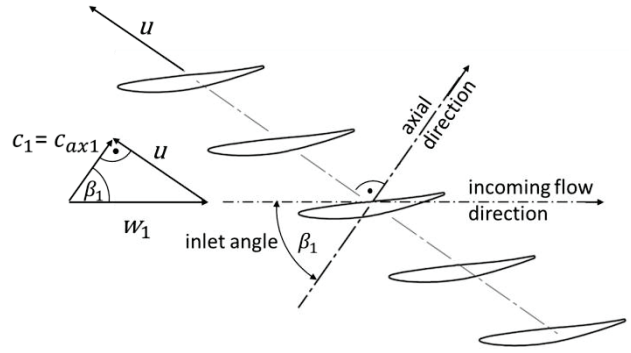

Fig. 10 Velocity triangle of the linear compressor cascade

The relative inlet velocity w_1 can be considered as the inlet velocity of the measuring section. This assumption requires, of course, a matching rotor blade speed u. In Fig. 10 the respective velocity triangle is depicted. The velocity triangle leads to:

(6) $tan\,\beta_1 = \frac{u}{c_{\mathrm{ax1}}}$

With equation (6) we describe the flow coefficient (see equation (3)) as follows:

(7) $\phi_1 = \frac{1}{tan\,\beta_1}$

For design conditions β_1 is the design inlet angle, respectively 55°. To include the off design case, the incidence angle i has to be added:

(8) $\beta_1 = 55° + i$

Finally, we describe the flow coefficient as follows:

(9) $\phi_1 = \frac{1}{tan(55° + i)}$

Hence, the flow coefficient is only a function of the incidence. With the turning of the circular plate the incidence is increased and the flow rate through the cascade is decreased.

5. EXPERMENTAL RESULTS AND DISCUSSION

The flow structures were visualized at various flow conditions. We varied tip clearance, angle of incidence, and Reynolds number. The essential results are achieved under flow conditions presented in Table 2. We distinguish between a low and a high Reynolds number and between a small and a large tip clearance at various angles of incidence. The incidence of 15° correlates e.g. with the flow coefficient Φ = 0.364. The tip clearance t is related to the chord length C.

incidence angle i	10°	15°	17,5°	20°	25°
$Re \approx 13000, t/C$=2%	x	x		x	x
$Re \approx 13000, t/C$=4%	x	x		x	x
$Re \approx 30000, t/C$=2%	x	x		x	x
$Re \approx 30000, t/C$=4%	x	x	x	x	x

Table 2 Investigated flow conditions

Fig. 11 shows the flow phenomena at the tip region of the cascade for a small tip clearance, an incidence of 10°, and

a low Reynolds number. Fig. 11 is composed of two parts. The upper part reveals a vertical view and the lower part reveals a horizontal view of the regarded area. The inlet boundary layer is visualized by blue inked fluid elements. The inlet boundary layer first splits because of the high pressure in front of the blades and then enters the passage. The inlet boundary layer moves to the suction side of the adjacent blade. The structure of the incoming boundary layer shows the good periodicity of the passages. A streakline crossing the tip clearance is visualized by green inked fluid elements. It can be seen that the inlet boundary layer interacts with the tip leakage flow, but they don't mix.

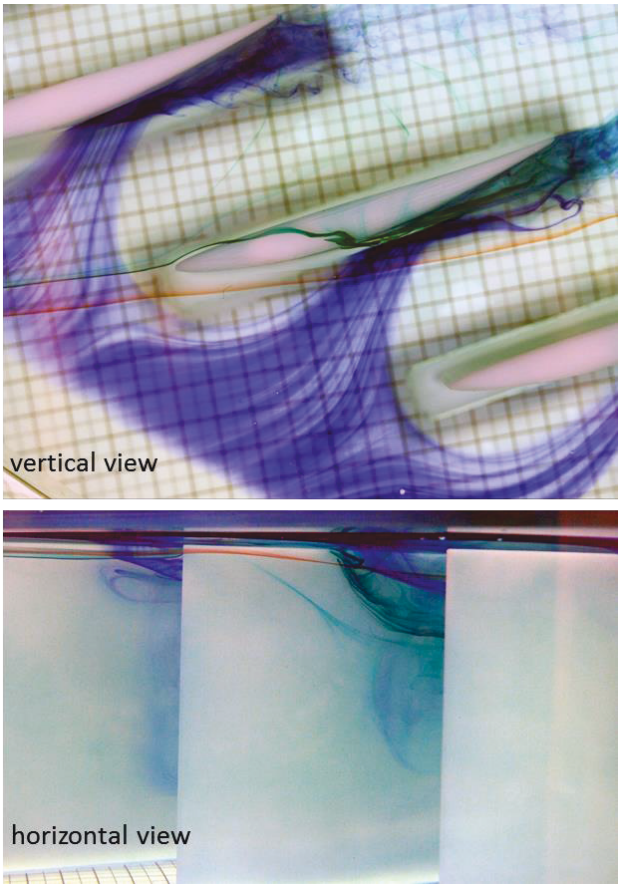

Fig. 11 Interaction of the incoming flow with the tip leakage flow (t/C=2%, i=10°, Re=14512)

Fig. 12 shows the interaction of the incoming flow with the tip leakage flow for an increased incidence of 15°. The Reynolds number is quit the same and the tip clearance is identical than in Fig. 11. The inlet boundary layer is visualized by blue inked fluid elements. It can be seen that the inlet boundary layer doesn't hit the suction side of the blades but detaches from the upper plate. The blockage of the inlet boundary layer is caused by the tip leakage flow. A streakline crossing the tip clearance is visualized by red inked fluid elements. It can be seen that the inlet boundary layer interacts with the tip leakage flow, but they don't mix. There is an interface zone between the incoming and tip leakage flow. Numerical studies also reveal an interface zone between the incoming flow and the tip leakage flow (see e.g. Vo [8]). By increasing the incidence, the interaction zone moves upstream.

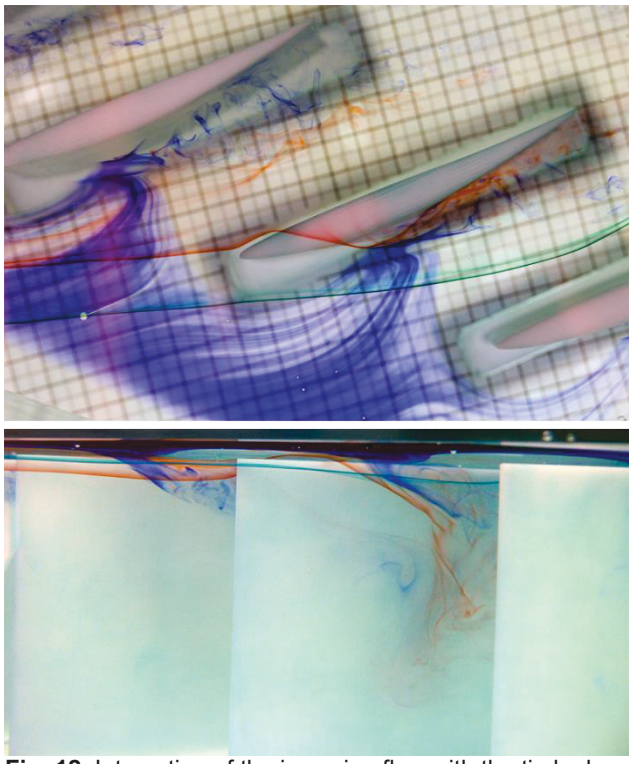

Fig. 12 Interaction of the incoming flow with the tip leakage flow (t/C=2%, i=15°, Re=13946)

The flow visualization presented in Fig. 13 was executed with a large tip clearance (t/C=4%). The Reynolds number is quit the same and the incidence is identical than in Fig. 12. The streakline crossing the tip clearance is visualized by green inked fluid elements. It can be seen that the direction of the tip leakage flow changes a little bit. The tip leakage rolls up into a vortex. The location of detachment of the incoming boundary layer is closely side by side to the position of rolling up of the tip leakage flow. However, it can be seen that the interaction zone moves downstream as a consequence of increasing the tip clearance.

The influence of tip clearance on the leakage flow direction is also shown in Fig. 14. These flow visualizations were executed by an incidence of 10° and a low Reynolds number. By enlarging the tip clearance from 2% to 4% chord, the angle δ between the chord and the tip leakage flow direction decreases. Therefore, by enlarging the clearance the origin of the leakage vortex moves downstream.

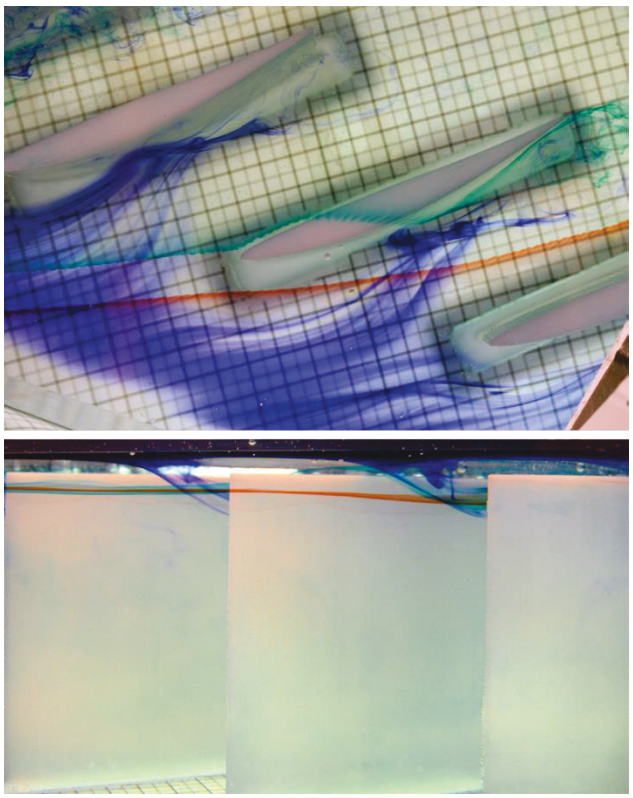

Fig. 13 Interaction of the incoming flow with the tip leakage flow (t/C=4%, i=15°, Re=12765)

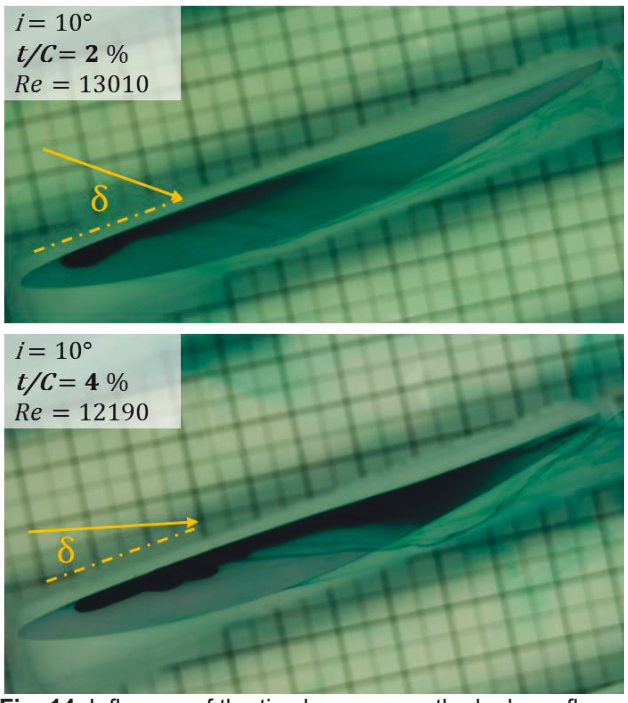

Fig. 14 Influence of the tip clearance on the leakage flow direction

Fig. 15 shows the flow phenomena at the tip region of the cascade for a high Reynolds number. The increasing of the Reynolds number is achieved by increasing the incoming velocity. The tip clearance and the incidence are the same than in Fig. 13. It can be seen that the interaction zone moves upstream as a consequence of increasing the Reynolds number. Also the origin of the leakage vortex moves upstream by enlarging the Reynolds number. Obviously, the pressure gradient between the pressure side and the suction side of the blade is changed by increasing the flow velocity in the measuring area.

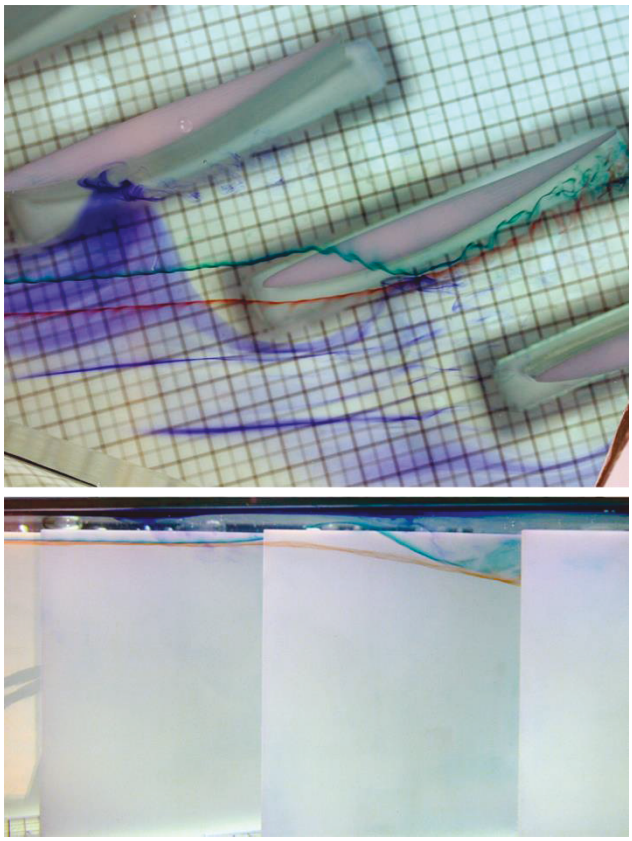

Fig. 15 Interaction of the incoming flow with the tip leakage flow (t/C=4%, i=15°, Re=26607)

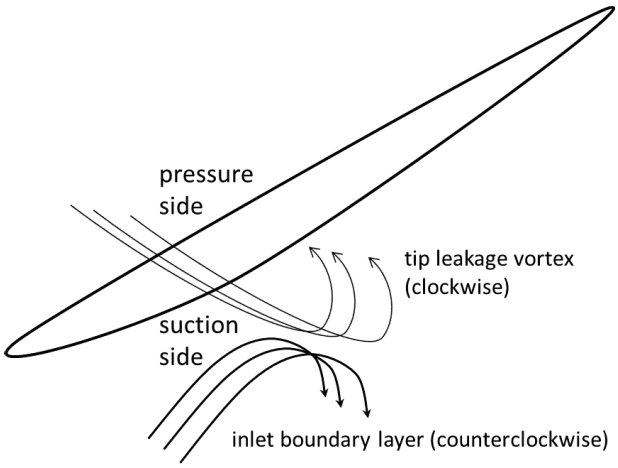

Fig. 16 Sketch of the interaction of the incoming boundary layer with the tip leakage flow

The observed interaction of the incoming boundary layer with the tip leakage flow is sketched in Fig. 16. The pressure gradient between the pressure and the suction side of the blade drives the tip leakage flow. The tip leakage flow as well as the incoming boundary layer rolls up into a

vortex. The tip leakage vortex rotates clockwise. The rolling up of the incoming boundary layer is counterclockwise. It has to be part of the horseshoe vortex system, which has a pressure side branch and a suction side branch [3, 12]. The suction side branch of the horse shoe vortex and the tip leakage vortex have the same direction of rotation. Besides, the suction side branch of the horse shoe vortex isn't so dominant than the pressure side branch of the horse shoe vortex. So it wasn't possible to observe this part of the horse shoe vortex. The rolling up of the incoming boundary layer is part of the pressure side branch of the horse shoe vortex.

In the following we regard only the two dominant vortex lines at inlet of the tip region of the passage. These are the tip leakage vortex and the pressure side branch of the horse shoe vortex. Both vortex lines proceed in the passage. The tip leakage vortex turns clockwise and the inlet boundary layer rolls up counterclockwise. So the vortex system in the passage consists of two neighboring vortices.

If a single vortex exists far away from any wall, it doesn't move. Two neighboring vortices, however, act at each other. The velocity field of the first vortex determines, the velocity of the center of the second vortex, and the velocity field of the second vortex determines the motion of the first. The resulting velocity can be thought of a superposition of the velocities of the two vortices. Two and more vortices influence each other and form a system that exhibits characteristic motions [14].

To calculate the flow characteristics of vortex lines of finite length, straight and curved, an exact analogy in the theory of electromagnetism, called the "Biot-Savart law" can be used. Applied to potential flow it is [14]:

$$(10)\quad \boldsymbol{v} = -\frac{\Gamma}{4\pi}\int\frac{\boldsymbol{r}\times d\boldsymbol{s}}{r^3}$$

For an infinitely long line the "point vortex" is [14]:

$$(11)\quad v = \frac{\Gamma}{2\pi r}$$

Zippel et al. has applied the Biot-Savart law to understand the motion of vortex systems in turbine cascades [15]. To understand the essential motion of a vortex system in turbine or compressor passages the vortices can be assumed to be parallel vortex lines. Dissipation has to be neglected and the vortices have to be considered as potential vortices. Hence, the vortices can be regarded in form of singularities like point vortices in a plane perpendicular to the main flow direction. Accordingly, equation (11) can be applied. A vortex near a wall can be mirrored on the wall [16]. So we get a symmetry plane instead of the wall and two symmetric vortices. For these vortices the Biot-Savart law can also be used.

These assumptions are applied to the vortex system in the compressor passage. The resulting potential vortex system is depicted in Fig. 17. Of course, the circulation Γ_L of the tip leakage vortex depends on the adjusted tip clearance and the pressure gradient between the pressure and the suction side of the blade. However, the circulation Γ_L of the tip leakage vortex is assumed stronger than the circulation Γ_H of the pressure side branch of the horse shoe vortex.

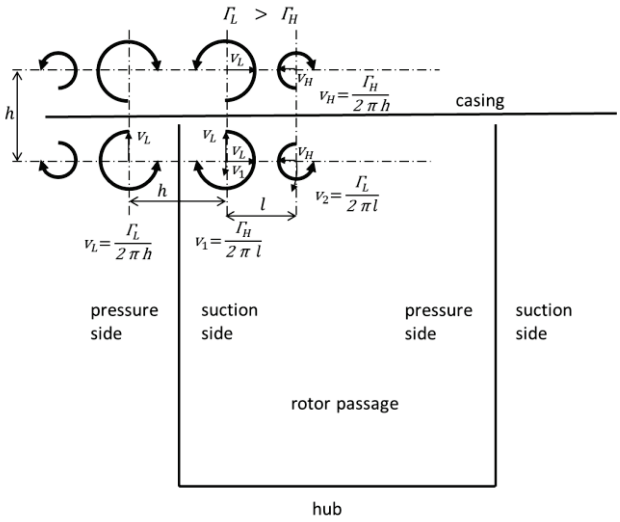

Fig. 17 Induced velocities on the dominant potential vortex system at the tip region of the passage

The movement of the tip leakage vortex is determined by the mirrored vortex on the blade, by the mirrored vortex on the casing, and by the neighboring horse shoe vortex. The movement of the horse shoe vortex is determined by the mirrored vortex on the casing, and by the neighboring vortex. The induced velocities are plotted at the centers of the rotation. Two vortices of equal strength but opposite rotation move forward on a straight line perpendicular to a line connecting the centers of the rotation. If the rotational velocities of the two vortices are different, the path of the system is curved towards the stronger vortex.

As the movement of the tip leakage vortex is blocked by the casing, the lip leakage vortex will move parallel to the casing towards the horse shoe vortex. The horse shoe vortex will also move towards the tip leakage vortex. Since the horse shoe vortex is weaker than the tip leakage vortex his path will be curved. As a result, the vortex system interacts in this way that they move against each other in which the horse shoe vortex shifts underneath the tip leakage vortex. In summary, the vortices form a consolidated system that move towards the middle of the passage. This may induce a partly blockage of the channel cross section. By reducing the flow coefficient, the tip leakage flow blockage will grow until the formation of spike rotation stall disturbances are most likely.

Reducing the flow coefficient can be realized at the water channel by increasing the incidence angle. Axial compres-

sors with low flow rate will often have large regions of separated flow. With low flow rate or high incidence the risk of instability arises. The outcome of instability will normally be stall but also surge could result. The most important aspect of compressor stall and surge is the prediction of the condition at which this will happen [13]. We found an incidence angle between 17.5° and 20° where instability arises. Of course, we cannot observe the inception of stall in the water channel. But at an incidence angle of 20° oscillations were observed in the flow. These oscillations give one of the origins to the phenomena of stall and surge.

The results presented so far are obtained in stable flow conditions. An example of instable operating of the linear cascade is shown by Fig. 18. The circular plate of the cascade was turned until the angle of incidence achieved 20°. The streakline crossing the tip clearance is visualized by green inked fluid elements and the incoming boundary layer by blue inked fluid elements.

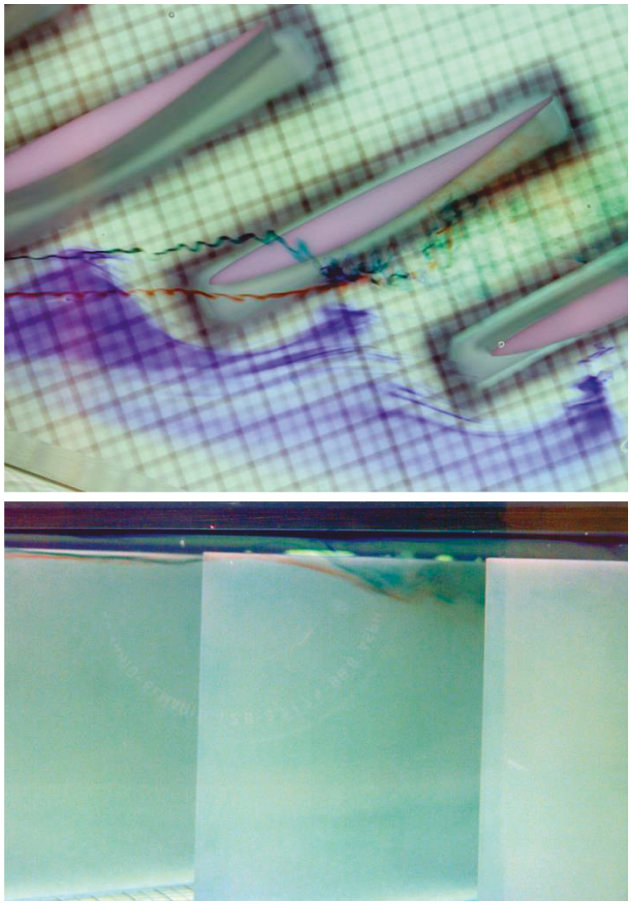

Fig. 18 Interaction of the incoming flow with the tip leakage flow (t/C=4%, i=20°, Re=30805)

The flow structures differ basically from the flow structures at stable operating conditions. A significant blockage of the passage was realized. The incoming boundary layer detaches already at the inlet of the passage and the tip leakage flow does not roll up into a vortex. Nevertheless, an area of interaction between the incoming boundary layer and the tip leakage flow can also be located. The tip leakage streakline enters this area, but then suddenly dissipates in a large recirculation zone.

Fig. 19 shows the interaction of the incoming flow with the tip leakage flow for an incidence of 25°. As the incidence was increased, compared to the flow study depicted in Fig. 18, also instable flow conditions are expected. It can be seen that the principle flow structures are the same. In spite of the increased inlet flow angle, the area of interaction remain at the same zone. Though, fluctuations of the flow interfere a precise determination of this zone. Also a change of Reynolds number and tip clearance do not change the principle structure of the tip flow region.

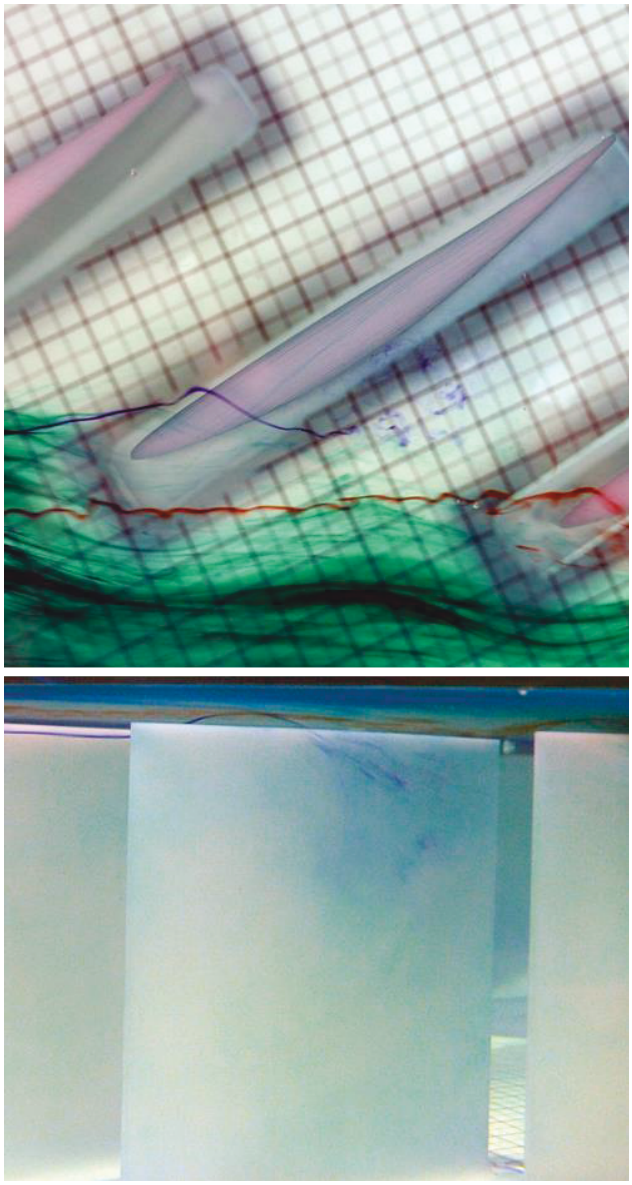

Fig. 19 Interaction of the incoming flow with the tip leakage flow (t/C=4%, i=25°, Re=30257)

In summary, we found that the stable flow conditions differ significantly from the instable flow conditions. At an incidence angle of 17.5° or lower all measurements were at stable flow conditions and at an incidence angle at 20° or

higher all measurements were at instable flow conditions. The incidence of 17.5° correlate with a flow coefficient of Φ=0.32 and the incidence of 20° correlate with a flow coefficient of Φ=0.28. Increased incidence means lower flow rate. A criterion for tip leakage blockage behavior, which is associated with spike stall inception, is not yet found in the water channel. The water channel results show, however, some similarity to the vortex breakdown phenomena found by Furukawa [10].

Quit recently, we have done first experiments with the Particle Tracking Velocimetry (PTV) in the water channel. So far, the experimental results with the Particle Tracking Velocimetry (PTV) confirm the visualization studies.

6. CONCLUSIONS

A detailed consideration of the interaction between the incoming boundary layer and the tip leakage flow is carried out. As the tip clearance rises, the tip leakage rolls up more intensely into a tip vortex and the position of the rolling up moves downstream. The tip clearance flow partly blocks the incoming flow and the incoming boundary layer detaches. The position of tip leakage rolling up and the position of detachment of the incoming boundary layer moves upstream under following conditions:

– reduced tip clearance width,
– increased angle of incidence,
– increased Reynolds number.

The location of detachment of the incoming boundary layer is closely side by side to the position of rolling up of the tip leakage flow regardless of gap width, incidence and Reynolds number. There is an interface between the incoming flow and the tip clearance flow. These characteristics are observed at stable flow conditions. The effect of instability generated by the tip leakage flow appears at an angle of incidence between 17.5° and 20°. The flow field under unstable conditions differs significantly from the flow field under stable flow conditions. The tip leakage fluid does not roll up into a tip vortex and the incoming boundary layer detaches already at the inlet of the passage under unstable flow conditions. Nevertheless, an area of interaction between the incoming boundary layer and the tip leakage flow can also be located. This systematic approach, with the focus on the area of interaction, provides a significant insight into the flow at the casing of a compressor cascade.

ACKNOWLEDGMENTS

A lot of the work reported here was done by three students. Mirijam Weimer helped to design the measuring section. Philipp Heimbucher and Alexis Papayannis undertook experiments. The authors would like to thank also Prof. Martin Rose who initialized the research.

References

[1] Storer, J. A., and Cumpsty, N. A., “Tip Leakage Flow in Axial Compressors,” *ASME Journal of Turbomachinery*, Vol. 113, 1991, pp. 252–259.

[2] Rains, D. A., “Tip Clearance Flows in Axial Flow Compressors and Pumps,” California Institute of Technology, Hydrodynamics and Mechanical Engineering Laboratories, 1954.

[3] Inoue, M., and Kuroumaru, M., “Structure of Tip Clearance Flow in an Isolated Axial Compressor Rotor,” *ASME Journal of Turbomachinery*, Vol 111, 1989, pp. 250–256.

[4] Inoue, M., Kuroumaru, M., and Fukuhara, M., “Behavior of Tip Leakage Flow Behind an Axial Compressor Rotor,” *ASME Journal of Engineering for Gas Turbines and Power*, Vol.108, 1986, pp. 7–14.

[5] Goto, A., “Three-Dimensional Flow and Mixing in an Axial Flow Compressor With Different Rotor Tip Clearances,” *ASME Journal of Turbomachinery*, Vol. 114, 1992, pp. 675–684.

[6] Fischer, A., Büttner, L., Czarske, J., Gottschall, M., Vogler, K., and Mailach, R., “Investigation of the Tip Clearance Flow in a Compressor Cascade Using a Novel Laser Measurement Technique With High Temporal Resolution,” *ASME Journal of Turbomachinery*, Vol. 134, 2012.

[7] Tan, C., S., Day, I., Morris, S., and Wadia, A., “Spike-Type Compressor Stall Inception, Detection and Control,” *Annual Review of Fluid Mechanics*, Vol. 42, 2010, pp. 275–300.

[8] Vo, H., D., *Role of Tip Clearance Flow on Axial Compressor Stability*, 2001.

[9] Hoying, D., A., Tan, C., S., Vo, H., D., and Greitzer, E., M., “Role of Blade Passage Flow Structures in Axial Compressor Rotating Stall Inception,” *ASME Proceedings*, 1998, pp. 98-GT-588.

[10] Furukawa, M., Inoue, M., Saiki, K., and Yamada, K., “The Role of Tip Leakage Vortex Breakdown in Compressor Rotor Aerodynamics,” *ASME Journal of Turbomachinery*, Vol. 121, 1999, pp. 469–480.

[11] Georgi J., Staudacher S., “Characteristics of Ejectors on Small Gas Turbine Engines,” *DLR Kongress*, Vol. 301339, 2013.

[12] Vogt, H., and Zippel M., “Sekundärströmungen in Turbinengittern mit geraden und gekrümmten Schaufeln; Visualisierung im ebenen Wasserkanal,” *Forschung im Ingenieurwesen*, Vol. 62, 1996, pp. 247–253.

[13] Cumpsty, N. A., *Compressor Aerodynamics*, Krieger Publishing Company, Malabar, Florida, 2004.

[14] Lugt, H. J., *Vortex Flow in Nature and Technology*, John Wiley & Sons, 1983.

[15] Zippel M., *Secondary Flow in Turbine Cascades, Multi-Vortex-Systems 1986 -1992*, 2015.

[16] Truckenbrodt, E., *Fluidmechanik Band 2: Elementare Strömungsvorgänge dichteveränderlicher Fluide sowie Potential- und Grenzschichtströmungen*, 1999.